Failure mechanisms of geosynthetic-reinforced wall with modular blocks: from centrifuge test to numerical analysis

C.G. Gragnano
Dept. of Civil, Chemical, Environmental and Materials Engineering, DICAM, University of Bologna, Italy (carmine.gragnano2@unibo.it)

ABSTRACT: The use of geosynthetics as structural elements in earthen wall stabilization is actually worldwide diffused and evaluation of reinforced soil retaining wall performance has rapidly become a fundamental problem in engineering works. Advanced numerical analysis in conjunction with experimental tests are usually required to perform accurate studies on the various failure mechanisms, as global instability, breakage of the reinforcements and pull-out failure. Built from results obtained on previous laboratory small-scale tests and preliminary numerical analysis, a real-scale finite element model of geosynthetic-reinforced soil retaining wall has been created mainly to investigate the structure performance respect to internal failure mechanisms, which study was not accounted during the experimental campaign conducted through centrifuge testing. For this purpose, geogrid tensile strength and soil-geogrid strength interface have been progressively, and separately, reduced until respective failures occur; afterwards, at different reduction degrees, safety analysis have been conducted in order to evaluate the residual strength state. This study aims to underline the influence of reinforcement resistance and soil-geogrid interaction parameters on internal stability evaluation. Furthermore, prelaminar indication on near-collapse conditions, in reference to breakage of the reinforcements and pull-out failure mechanisms, are finally provided.

Keywords: Numerical modelling, geosynthetic-reinforced soil wall, geogrids breakage, pull-out failure

1 INTRODUCTION

Improvement on the use of geosynthetics as soil reinforcement in civil engineering works is a topical research field involving various geotechnical issues. Referring to mechanically stabilized earth walls, design practice requires safety condition statements respects to limit states both for internal and external modes of failure. As support to the standard practice, experimental and numerical studies have been frequently conducted in the last two decades aiming to reach an exhaustive comprehension of the reinforced soil performance for several configuration and stress conditions, reproducing different stages of the structure service life (Cai and Bathurst, 1995; Allen et al., 2003; Ling and Leshchinsky, 2003; Hatami and Bathurst, 2005; Huang et al., 2009; Ling and Liu, 2009; Yang and Annamraju, 2013; Yu et al, 2016).
Aiming to enhance the current knowledge on geosynthetic-soil interaction mechanisms and to pursue previous works achievements, a Finite Element numerical study has been conducted starting from results obtained on laboratory tests and preliminary analysis. In specific, a set of

centrifuge tests on small-scale geosynthetic-reinforced soil retaining structures with modular block facing was carried out at the Geotechnical Laboratory of the Columbia University, in order to investigate the influence of a number of design parameters, such as length and vertical spacing of the reinforcement layers on the wall behavior under increasing gravity loading; detailed description of the testing facilities as well as of the laboratory models construction can be found in Iacorossi et al. (2013). A series of numerical analysis, using a finite element approach with two alternative elasto-plastic constitutive model characterized by a different degrees of sophistication, were further performed in order to underline the need to use an advanced formulation to faithfully reproduce the response of the small-scale geosynthetic-reinforced wall from centrifuge tests, focusing on a suitable backfill modeling and a proper description of interface effects (Gottardi et al., 2014), achieving a good predictive model. Nevertheless, due to the particular load path followed, both small-scale laboratory tests and numerical analysis mentioned above only investigated global failure mechanism, finding that a reinforcements length of 40% the wall height provides a fully stable response in absence of additional external load.

Using the hardening elasto-plastic constitutive model for the backfill and the best set of parameters identified in Gottardi et al. (2014) and starting from data collected by means of the centrifuge testing program (Iacorossi, 2012), real-scale finite element models of geosynthetic-reinforced soil retaining structure have been now created to obtain a more complete description of the wall behavior under static loading, to confirm the results obtained by the previous study and to explore other collapse mechanisms, i.e. breakage of the reinforcements and pull-out failure. Results hereafter presented mainly focus on internal failure mechanisms and soil-reinforcement interaction for a mechanically stabilized earth (MSE) wall with level backfill and no external surcharge.

2   INTERNAL FAILURES FOR MSE WALLS

Internal failure of a mechanically stabilized earth wall directly involves reinforcement elements, frequently leading to loss of serviceability and possible collapse of the whole structure. Usually, the principal mechanisms to which internal instability refers are geogrids breakage and pull-out failure, occurring when the tensile forces in the reinforcement layers become larger than the specific resistances. Internal stability evaluation still represents a fundamental part of the assessment and designing process, where the determination of the maximum developed tensile forces, their location along a critical slip surfaces and the resistance provided by the reinforcements, during the short and long term period both in tensile strength and pull-out capacity, are necessarily required.

The tensile forces are strictly dependent on the stress transfer between the soil and the reinforcement, taking place continuously along the geogrid trough friction and passive resistance, depending on geometry, on soil and reinforcement properties and their interaction mechanisms. Friction develops when there is relative shear displacement between soil and the reinforcement surface; passive resistance occurs through the development of bearing stress on transverse geogrid surfaces normal to the direction of soil-reinforcement relative movement. Using the National Highway Institute (NHI, 2009) simplified method for MSE wall under soil self-weight loading and level backfill, the maximum reinforcement tensile load, T_{max}, can be computed as:

$$T_{max} = S_v \gamma_r (H - z) K_r \qquad (1)$$

where S_v = vertical reinforcement spacing, γ_r = unit weight of soil in the reinforced zone, H = height of the wall, z = height of the reinforcement level from the bottom of the wall, and K_r is the coefficient of mobilized lateral stress in the reinforced soil zone; for extensible (e.g. geosynthetics) and continuous reinforcement, K_r is assumed to be equal to the minimum earth pressure coefficient (K_a), meaning that, for internal stability design, the critical slip surface in

a reinforced wall is assumed to coincide with the locus of the maximum tensile forces, T_{max}, acting in each reinforcement layer. The determination of the shape of the predicted critical failure surface is based upon instrumented structures and theoretical studies and is primarily related to the type and geometry of reinforcement (Allen et al., 2001); as suggested by the NHI guidelines (2009), for internal stability design, the critical failure surface can be assumed to be linear in the case of extensible reinforcements passing through the toe of the wall, and its location defines, in turns, the embedment length in the resisting zone, L_e. For MSE walls with extensible reinforcement, vertical face and horizontal backfill, as the considered study case, L_e can be estimated as:

$$L_e = L - z \cdot tan(45 - \phi'/2) \qquad (2)$$

where L = total reinforcement length, and ϕ' = effective friction angle of retained backfill. Therefore, design stability with respect to pull-out of the reinforcements requires that the effective pull-out length is greater than or equal to the tensile load in the reinforcement so that the following criteria should be satisfied:

$$L_e \geq \frac{T_{max}}{F^* \alpha \gamma_r (H-z) C R_C} \qquad (3)$$

where α is the scale correction factor, equal to 0.8 for the considered cases, C depends on the reinforcement type, equal to 2 for strips and grids, and R_C is the coverage ratio, equal to 1 for continuous reinforcement. Pull-out resistance of the reinforcement is mobilized trough one or a combination of the two basic soil-reinforcement interaction mechanisms, interface friction and passive soil resistance, and can be estimated using simplified or advanced approach largely discussed in literature (Moraci and Gioffrè, 2006; Bathurst et al., 2012; Jacobs et al., 2014), however the best design approach is to carry out pull-out test under service levels of confining stress (Siera et al., 2009). The soil-to-reinforcement relative movement, required to mobilize the design tensile force, mainly depends upon the load transfer mechanisms, the extensibility of the reinforcement material, the soil type and the confining pressure; besides, the long term pull-out performance is predominantly controlled by the creep characteristics of the soil and the reinforcement materials.

Strength properties of geosynthetic reinforcement are, then, determined considering all possible time-dependent strength losses over the design life period, including installation damage, aging, temperature and confining stress, which reduce the ultimate geosynthetic tensile strength, T_{ult}, to the available long term strength, T_{al}. For preliminary design of permanent structures, the long term tensile strength, T_{al}, may be evaluated dividing T_{ult} by a factor equal to 7; this value has been established by multiplying lower bound reduction factors obtained from currently available test data on geosynthetic reinforcement, for products which meet the minimum requirements for use defined by the National Highway Institute; for temporary applications not having severe consequences, a default value for reduction factor of 3.5 rather than 7 may be considered. (3.5.2g Preliminary Design Reduction Factor, NHI, 2009).

3 NUMERICAL MODEL

The need to have stress similarity between the small-scale and the real-scale models plays a fundamental role in centrifuge tests interpretation and the choice of a proper scaling law is a key aspect for the truthfulness of the results hereafter presented. The main difficulty is related to how acceleration is applied trough the centrifuge; in the field, the Earth gravity is uniform trough the depth of the soil; differently, performing a centrifuge test there is a slight variation of inertial acceleration trough the small-scale model depending on the radius of the generic element in rotation. Actually, this problem turns out to have a minor effect when care is taken

to choose the radius at which the acceleration has to be determined. Therefore, a linear scaling law has been adopted to switch from small-scale to real-scale model, leading to almost negligible error. In particular, since the centrifuge tests were conducted up to acceleration equal to 35 g, all small-scale model geometrical data have been multiplied by 35, obtaining a 5-meter height reinforced soil retaining wall and facing blocks each characterized by 0.38 m x 0.77 m x 0.52 m dimensions.

The real-scale geosynthetic-reinforced retaining wall has been modelled using the finite element program PLAXIS 2D; advanced constitutive formulation referred as Hardening Soil Model (HSM, Schanz et al., 1999) and Mohr-Coulomb failure criterion have been considered for the backfill, a fine uniform sand which main physical properties are reported in Table 1. The soil behavior is so defined by isotropic elasticity using a highly nonlinear stress-dependency of soil stiffness for primary loading and unloading-reloading stress paths, as a function of the effective stress and strength parameters. The HSM is, then, characterized by two yield surfaces which evolve isotropically: a shear hardening yield surface that is a function of the deviatoric plastic strain and a cap yield surface which is introduced to bound the elastic region for compressive stress paths and depends on the plastic volumetric strain. In the present work, the elastic region of the models has been further reduced by means of a tensile cut-off.

Table 1. Backfill physical properties

D_{50} (mm)	Specific gravity	Dry unit weight of soil (kN/m³)	Relative density (%)	Gravimetric water content (%)
0.15	2.67	16	90	5.0

The fiberglass mesh coated in polymeric film, used as reinforcement in the small-scale centrifuge test, has been simulated trough elasto-plastic geogrid elements that can only sustain tensile forces, described by an elastic normal stiffness EA and a tensile strength, T_{ult}, respectively equal to 10.74 kN/m and 474.5 kN/m; these values, obtained through tensile tests performed on a few 20L x 5W cm specimens, were used in the numerical FE model. Retaining wall foundation has been modelled through the use of elastic isotropic plate element. A linear elastic behavior was also assumed for the facing blocks. Geogrid and material mechanical properties values are listed in Table 2.

Table 2. Geogrid and material properties used in the FE analyses

Geogrid tensile strength (kN/m)	Elastic normal stiffness (kN/m)	Effective friction angle (°)	Effective cohesion (kPa)	Dilatancy angle (°)	Poisson's ratio (-)
10.4	474.5	39.4	1.5	7.0	0.2

Interface element was added to geogrid, facing blocks and foundation plate for a proper modelling of soil-structure interaction. The material properties of the interface elements, reported in Table 3, have been defined from the parameters assumed for the adjacent soil and the roughness of the interaction is modelled by choosing a suitable value for the interface strength reduction multiplier, R_{int}; this factor relates the interface strength to the adjacent soil strength by applying the following rules:

$$c'_{int} = R_{int}c'_{soil} \qquad tan\phi'_{int} = R_{int}tan\phi'_{soil} \leq tan\phi'_{soil} \qquad \psi_{int} = 0° \text{ for } R_{int} < 1$$

A further interface was added to model the block-block interaction, which was supposed to be intermediate between smooth and fully rough, being the aluminum blocks infilled with sands.

All described properties refer to the best set of parameters identified in Gottardi et al. (2014), where special attention was focused not only on the modelling of the sand backfill, but also on the proper description of interface effects using an advanced constitutive formulation, which represent a crucial point for the accuracy of the numerical model outcomes, as also discussed in Yu et al. (2015).

Table 3. Interfaces properties used in the FE analyses

E_{50}^{ref} (MPa)	E_{oed}^{ref} (MPa)	E_{ur}^{ref} (MPa)	R_{int} block-block (-)	R_{int} soil-geogrid (-)	R_{int} soil-block (-)
16.4	16.4	49.2	0.5	0.7	0.42

The adopted mesh, consisting of 15-node triangular elements, together with the structural components included in the numerical model is given in Figure 1 with reference to a reinforcements length of 70% of the wall height. The picture shows that interfaces were generally extended beyond the end of structural elements, according to the procedure suggested in the PLAXIS 2D Reference Manual (Brinkgreve et al., 2011). The construction sequence was simulated incrementally, according to the experimental procedure described in Iacorossi (2012).
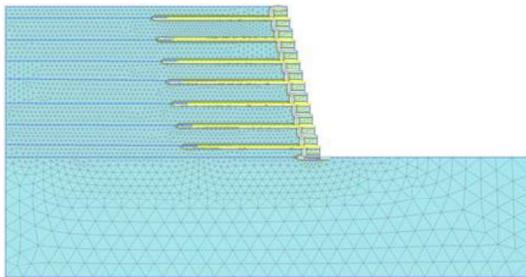
Figure 1: Finite element mesh adopted for the real-scale numerical model

Numerical analyses have been, then, conducted on different reinforcement configuration; length and vertical spacing of the geogrids have been chosen according to recommendation typically provided in design guidelines (e.g. by the NHI, 2009; AASHTO, 2010). Two different reinforcement lengths, 3.5 m (L7) and 4.5 m (L9), expressed as percentage of the wall height (70% and 90%, respectively) and two different spacing configurations, S2 and S1, defined in terms of block units between each reinforcement layer (two and one block spacing, respectively), were considered. Throughout, three geosynthetic-reinforced soil configuration were modelled: L7S2 as first, L9S2 and L7S1 then, aiming to assess the influence of reinforcements length and spacing on the internal failure mechanisms.

4   RESULTS AND DISCUSSION

To investigate the retaining wall performance in reference to breakage of the reinforcements and pull-out failure through the FE numerical models, geogrid tensile strength and soil-geogrid interface strength have been progressively, and separately, reduced in plastic analysis until failure of the structure occurs. In details, starting from the equilibrium phase reached at the end of the simulated construction process, a first set of numerical analysis have been performed on the three studied configurations (L7S2, L9S2, L7S1) assuming decreasing values for T_{ult}, equal to 75%, 50%, 25% and 12.5% (whether possible) of the initial case; whether equilibrium was not reached at one of the above mentioned stages, further analysis have been performed in order to find the lowest value of T_{ult} for which plastic analysis could be fully performed, in near collapse conditions for geogrids breakage. Afterwards, at all considered T_{ult} reduction stages,

safety calculations have been conducted in order to evaluate the residual strength states, using the φ' − c' reduction procedure (Brinkgreve et al., 2011), where soil, interfaces and structural element (e.g. geogrid) strength parameters are successively reduced by the same factor, until failure occurs; this factor is defined as:

$$\Sigma M_{SF} = \frac{available\ strength}{strength\ at\ failure} \qquad (4)$$

where ΣM_{SF} is the total multiplier used to define the value of the soil, interfaces and structural strength parameters at the last calculation step in the analysis. Similar procedure has been used to study pull-out mechanism, progressively decreasing soil-geogrid interface strength R_{int} for the interface elements up to failure conditions and performing various safety calculations.

4.1 Geogrids breakage failure mechanism

The first considered internal mode of failure is local breakage of reinforcement elements, reached progressively reducing geogrid tensile strength T_{ult} in subsequent plastic analysis; in Figure 2 are presented two representative results of geogrids breakage failure for the L7S2 (left) and L9S2 (right) configuration. Showed data are collected for T_{ult} equal to 32% of the initial value, that is the lower values for which equilibrium is reached, considering L7S2 configuration. In specific, Phase total displacements, Pu, are plotted in Figure 2a and Phase deviatoric strains, $P\gamma_s$, in Figure 2b, both for soil and structural element. The appellative "Phase" denote that the considered output refers to their differential values between the end of the current calculation phase and the end of the previous calculation phase. In this case, the Pu and $P\gamma_s$ are displacements and deformations occurring reducing T_{ult} from 50% to 32% of the initial value, and are considered to be significant to point out the incipient collapse.
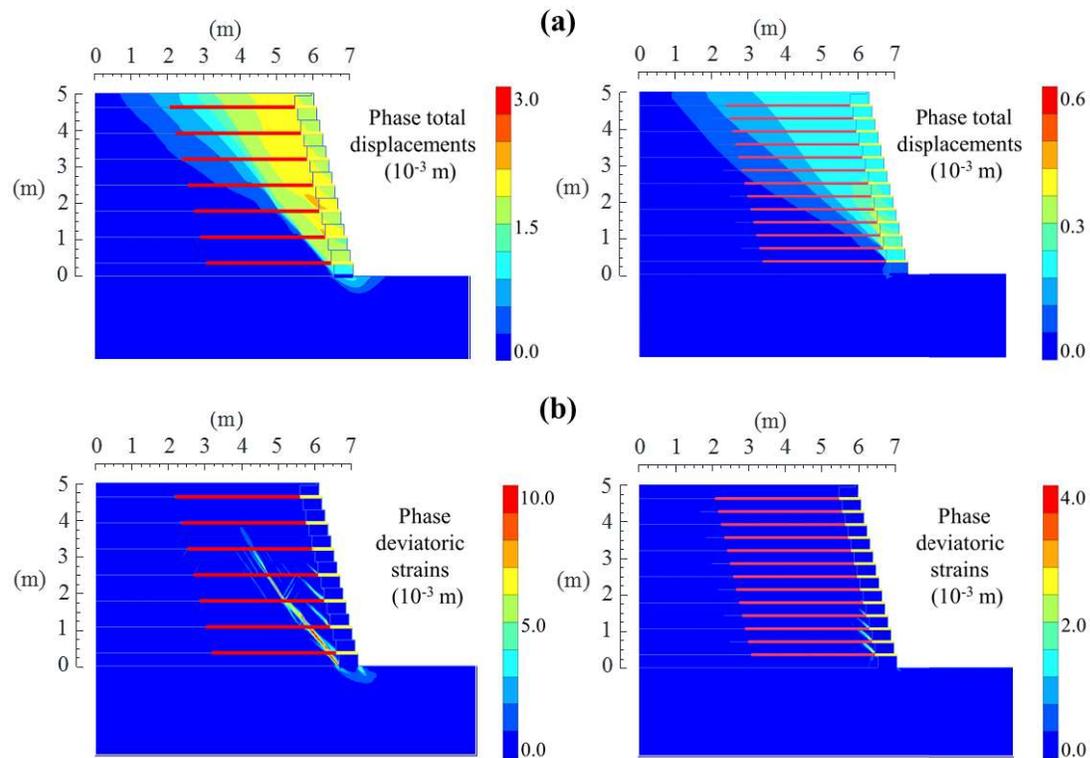
Figure 2: Numerical results from analysis performed to investigate geogrids breakage failure mechanism for L7S2 (left) and L7S1 (right) configuration: Phase total displacements Pu (a) and Phase deviatoric strains $P\gamma_s$ (b) evaluated decreasing geogrid tensile strength T_{ult} from 50% to 32% of the initial value

Firstly, it has to be noticed that different limit scale values were used, in order to properly display all deformation paths. In particular, Pu and $P\gamma_s$ scale amplitudes differ by a ratio of 5 and 2.5, respectively, between the two configuration. This mainly denote the strong difference existing between maximum displacements and the deformations reached for the showed cases, which is of approximately one order of magnitude. Besides, of great importance appear the stability conditions in relation to geogrids breakage failure: L7S2, for the specific T_{ult} reduction stage, is approaching collapse state, evidencing significant values of deviatoric strains, locating an internal critical slip surface in correspondence of the breakage of the reinforcements. In contrast, L7S1 configuration appear relatively far from the critical state for the considered value of T_{ult}, as mean of the a more widespread presence of reinforcing elements in the backfill reducing geogrids damages, that will be clearly evidenced only decreasing reinforcement strength up to 12.5% of the initial value, and providing a safety margin nearly three times respect the L7S2 case, for the considered mechanism and stress condition. Moreover, in Figure 3 are plotted the Phase horizontal displacements, Pu_x, reached at the end of safety calculations in failure conditions, for geosynthetics located at different heights from the bottom of the wall for L7S2 (left) and L7S1 (right) configuration.
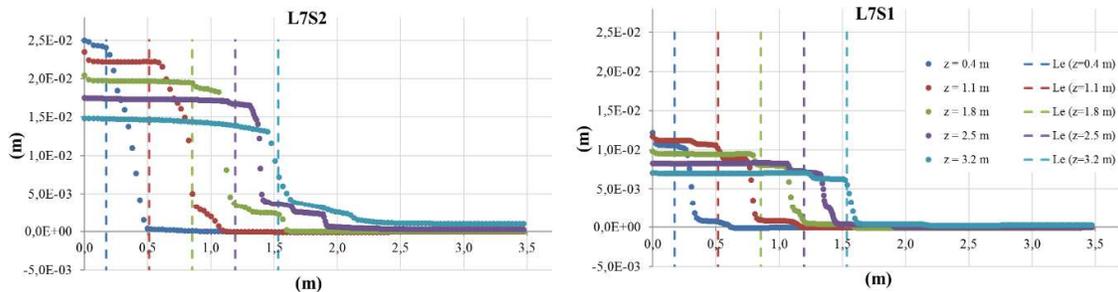
Figure 3: Phase horizontal displacement, Pu_x, computed in failure conditions for geosynthetics in L7S2 (left) and L7S1 (right); each reinforcement layer is identified by its height from the bottom of the wall. In dashed lines are plotted the lengths of the embedment, L_e, in the resisting zones, estimated following NHI (2009) recommendations.

Horizontal displacements are mainly distributed along the geogrids until breakage, beyond which there is a stable area, mainly dependent on the embedded geogrid length and confining pressure. This is clearly evident both for the L7S2 and L7S1 MSE walls, where a unique and well-defined internal critical slip surface could be identified in failure conditions. Nevertheless, the location of the internal critical slip surfaces in near collapse conditions for the two configurations seems to be not affected by just by the vertical spacing of the reinforcement layers. Together with horizontal displacements, in Figure 3 are showed the embedment lengths in the resisting zone, L_e, computed using equation 2; in detail, dashed lines also identify the location of the critical slip surface according to the formulation provided by the NHI guidelines (2009). Analytical and numerical predictions seem here to be in good agreement, particularly considering the overall location of the unstable area identified by the critical slip surfaces; however, it can be noticed that NHI suggestion generally tends to provide slightly higher values for the embedded lengths, therefore less conservative results for the considered cases, respect to those estimated trough FE analyses. These findings can be mainly ascribed to the different shapes of the critical slip surfaces estimated using numerical analysis and the ones assumed for the analytical method, which are found to be highly nonlinear and linear, respectively. Furthermore, it is here useful to notice that the Load and Resistance Factor Design (LRFD) method is not been considered in analytical formulations for the L_e calculation.

4.2 *Pull-out failure mechanism*

In separate numerical analysis, pull-out failure mechanism has been studied progressively reducing soil-geogrid interface strength, R_{int}; results are given in Figure 4 in terms of Phase total

displacements, Pu (a), and Phase deviatoric strains, $P\gamma_s$ (b), for the L7S2 (left) and L9S2 (right) configuration.

These data are plotted using the same graphic scale for each output and refer to a R_{int} reduction stage of 21% of the initial value, which represents the limit interface strength condition for which equilibrium can be reached for L7S2 configuration.
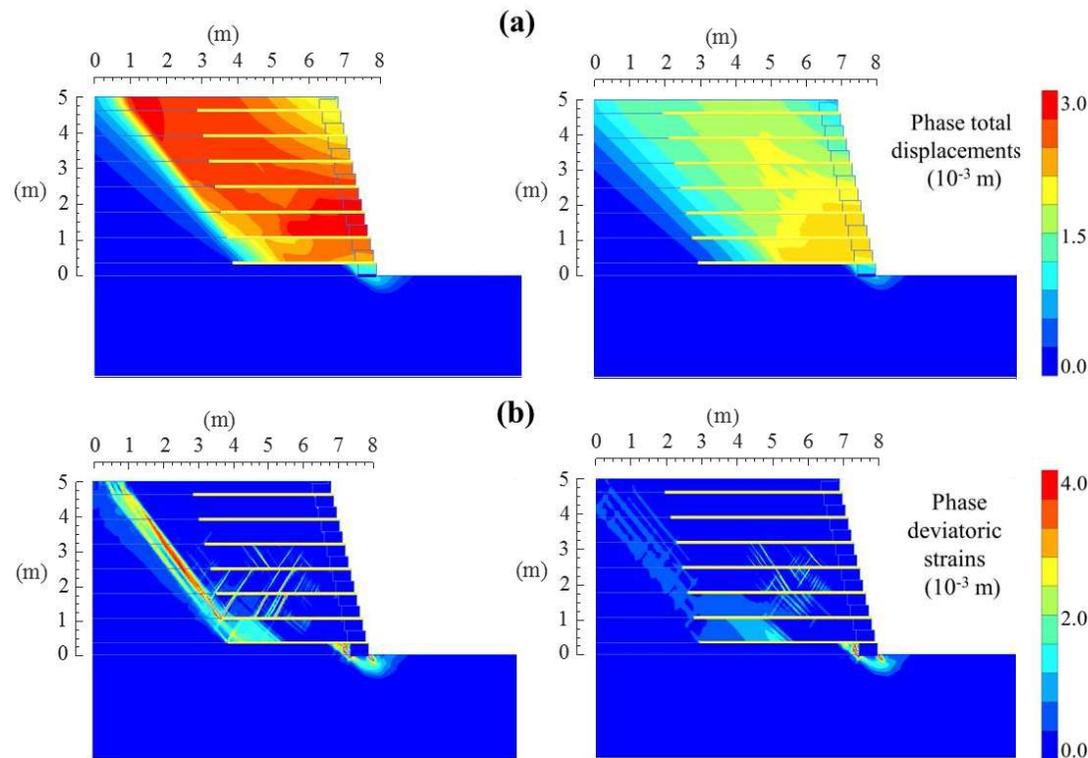
Figure 4: Numerical results from analysis performed to investigate pull-out failure for L7S2 (left) and L9S2 (right) configuration: Phase total displacements Pu (a) and Phase deviatoric strains $P\gamma_s$ (b) evaluated decreasing soil-geogrid R_{int} from 25% to 21% of the initial value

The above showed output show that, for the same strength decreasing path and soil-geogrid R_{int}, the L9S2 configuration appear to be more stable than L7S2. In particular, the deviatoric strains evidence a fully developed critical surface completely involving the L7S2 retaining wall, which tends to entirely slip to the right. The extended reinforcement lengths of L9S2 tends to guarantee a larger embedded zone and delay the collapse occurrence, that is reached for a soil-geogrid R_{int} equal to 15% of the initial value, achieving a remarkable increase in terms of safety respect to pull-out failure. Indeed, the two model do not significantly differ for the magnitude of the maximum value of Pu reached, equal to 0.0029 m for L7S2 and 0.0024 m for L9S2; however, an important difference lies in the homogeneity of the maximum phase total displacement distribution in LS72, involving all the retaining structure, differently from L9S2, where the maximum phase displacements are reached at the lowest geogrid layers. In Figure 5 are then showed axial forces, N, acting in the reinforcement. In specific, these results were obtained from plastic analysis performed in near collapse condition for L7S2 (left) and L9S2 configuration (right), at different R_{int} values, reduced until failure occurs: plotted data refer to reinforcement layers at 2.5 m and 0.4 m heights from the bottom of the wall. When soil-geogrid interface strength is fully available, the higher values for axial stresses are only nearby the connection zone, and tend to rapidly reduce with length. In this conditions, the maximum horizontal displacements of the geogrids are achieved only in proximity of the wall, while the remaining part of the reinforcements lies in the embedded zone, so that the resistance is fully mobilized only in a limited area. Besides, for R_{int} values reduced up to 0.35 (50% of the initial

value), the plotted data are almost overlapped, so that no stress redistribution is needed to en-sure equilibrium, meaning that only a small part of the displacements reached in failure condi-tions have already occurred. The effect of progressive reduction in R_{int} is to trigger pull-out instability so that horizontal displacement rapidly increases at soil-geogrid interfaces in near collapse condition; as consequence, axial forces are redistributed for a longer part of the ge-ogrids and the available resistance is almost fully mobilized, even if is significantly lower than the initial value.
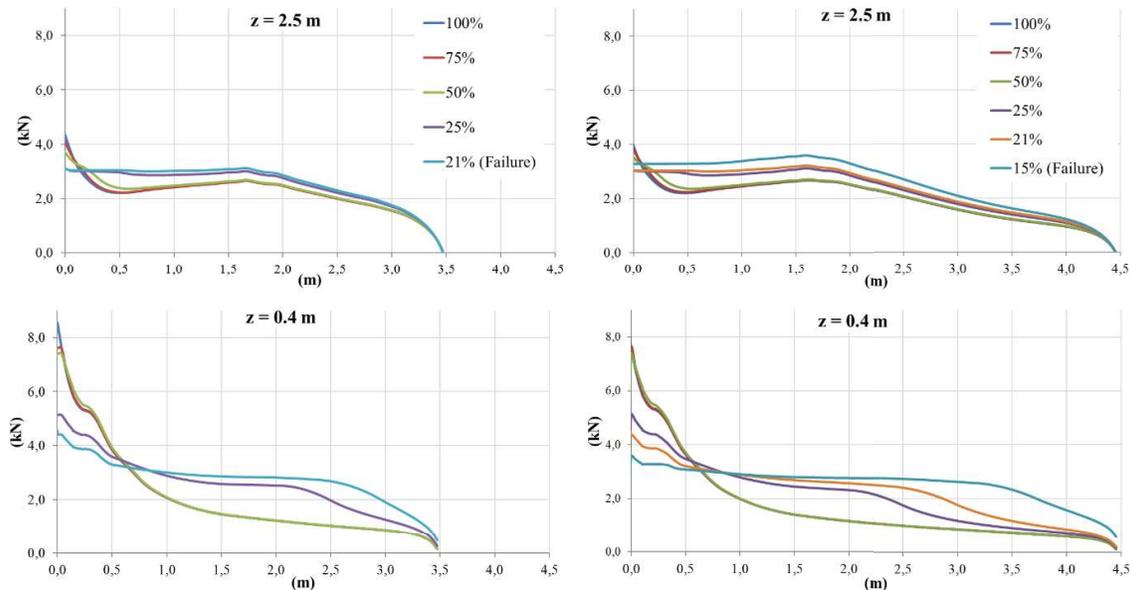
Figure 5: Axial forces, N, computed in failure condition for L7S2 (left) and L9S2 (right) configuration for reinforcement layer a 2.5 m and 0.4 m from the bottom of the wall; in dashed lines are plotted the length of the embedment in the resisting zone, L_e, estimated following NHI (2009) design recommendations

The observed mechanism, even if defined for a specific load path, can be also representative for other site conditions, as time-dependent strength losses, or could also reproduce different stress condition, e.g. increasing of the external loads, similarly leading to the complete interface strength mobilization. In general, these results show the importance of choosing a suitable re-inforcements length for avoiding pull-out failure, for which expected stress and deformation conditions should be carefully evaluated, eventually, using suitable numerical simulations, and highlight that geosynthetic elements need to follow a particular stress-strain path to fully mo-bilize the available interface strength.

4.3 *MSE wall safety condition*

In order to study the evolution of stability condition, safety analysis have been performed at all considered stages using the $\varphi' - c'$ reduction procedure (Brinkgreve et al., 2011). Global safety factors are given for the different configurations in terms of ΣM_{SF}, previously defined in equa-tion 4, and showed in Figure 6. Plotted data point out the safer stability conditions achieved reducing the vertical reinforcement spacing (L7S1), especially considering geogrids breakage failure; furthermore, an increase of geogrids length (L9S2) provide a more resistant MSE wall configuration respect to pull-out failure, even with less appreciable benefit regarding breakage of the reinforcements. As also above mentioned, it should be here noted that in safety analysis, all soil, interfaces and geogrids strength properties are reduced until equilibrium is not guaran-teed and global failure conditions are reached; therefore, these values do not represent the safety factor towards an individual mechanism but, more in detail, the residual strength states

of the structure, depending on the initial conditions and the specific stress-strain paths. It appears so justified that ΣM_{sf} values are found to be not higher than 1.9, and significantly lower than the usual safety factors for internal and external stability modes of failure for similar reinforced-soil wall configurations and stress conditions (Allen et al., 2002).
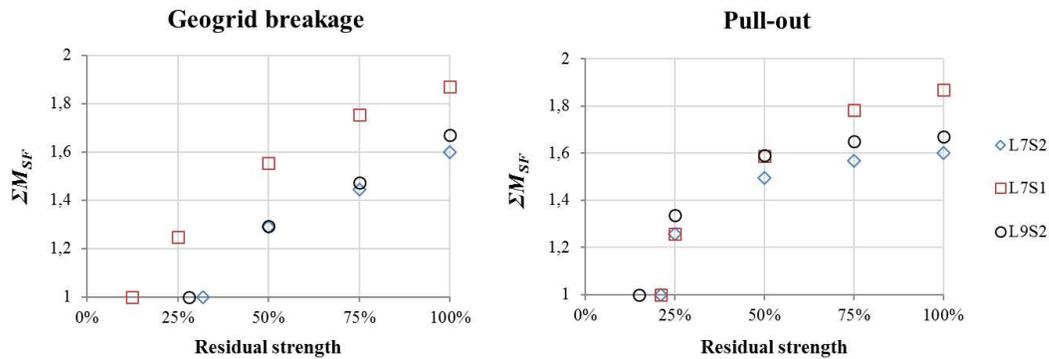
Figure 6: ΣM_{SF} reached value in safety analysis performed starting from T_{ult} (left) and R_{int} (right) strength values reduced respect the initial value

The maximum reduction factors, RF, here defined as the highest values for which the initial strength parameters were divided, i.e. the inverse values of the least R_{int}, are then listed in Table 3 for all considered cases.

Table 4. Reduction factors and total horizontal displacement from numerical analysis

	Pull-out			Geogrid breakage		
MSE wall	L7S2	L7S1	L9S2	L7S2	L7S1	L9S2
RF (-)	4.8	4.9	6.7	3.1	8.0	3.6

Compared to ΣM_{SF}, RF values could be more consistently referred as safety factor for the specific internal failure and stress conditions, representing the highest ratio between initial and residual strengths for each mechanism. These results clearly demonstrate, and confirm, the strong influence of reinforcements S_v on geogrids breakage mechanism and, otherwise, the effect of increasing reinforcements length to limit pull-out occurrence. For means of comparison, the safety factors for internal stability with respect to pull-out failure, expressed as the ratio between the available resistance and load evaluated following NHI (2009) suggestion and equations (1) to (3), have been evaluated, finding to be equal to 5.7, 7.4 and 9.8 respectively for L7S2, L7S1 and L9S2 configuration, resulting generally higher than the reduction factors estimated through numerical analysis. Anyhow, a similar consideration cannot be properly verified for geogrid breakage failure, for which would be required additional information about creep and durability properties on geosynthetics and accurate experimental testing; however, for preliminary design, it's worth to notice that the available long term strength may be evaluated without product specific data assuming a reduction factor equal to 7 (NHI, 2009), resulting more conservative only compared to L7S1 numerical results. It should be noted that the total RF suggested by NHI may be reduced significantly with appropriate test data. It is, in fact, not uncommon for products with creep, installation damage and aging data to develop total RF in the range of 3 to 6, or even less, with the development of new materials.

5 CONCLUSIONS

This paper presents and discuss the results of a FE study on different real-scale geosynthetic soil-reinforced retaining wall configurations; soil and interface parameters calibration here adopted have been carefully studied using data obtained on a previous experimental campaign, conducted by means of laboratory small-scale tests performed in centrifuge, and preliminary numerical analysis, performed through FE approach considering two alternative elasto-plastic constitutive model characterized by a different degrees of sophistication. Main purpose of this works is to study and to reproduce the internal failure modes for a geosynthetic-reinforced wall with modular blocks, in specific geogrid breakage and pull-out, describing the mechanisms involved and the influence of design parameters, as vertical spacing and reinforcement length, on stability conditions. Plastic analysis have been performed progressively reducing, in separate calculations, strength parameters for the considered failure mechanism, i.e. the ultimate geosynthetic tensile resistance and soil-geogrid strength interface, under soil self-weight loading. Obtained results clearly shows that vertical spacing and reinforcements length have their major impact on avoiding geogrid breakage and pull-out mechanisms, respectively, but have limited effects on the other mode of failure. Main findings and observations above discussed could, however, be extended to other stress-strain path leading to the same collapse mechanisms, as reinforced element degradation as effect of installation damage, chemical degradation, aging and/or creep resulting from long-term sustained tensile applied load, providing prelaminar indications to be used in standard engineering practice. Even if this study has been restricted to internal failure modes, numerical modeling appears a powerful tool for design and stability assessment of geosynthetic-reinforced soil retaining structures, being able to catch the full-scale MSE wall behavior respect to internal modes of failure, and providing realistic values for stress and strain distribution, although experimental tests are needed to accurately calibrate and validate numerical parameters and results.

REFERENCES

American Association of State Highway and Transportation Officials (AASHTO). 2010. LFRD bridge design specification. 5th Ed., AASHTO. Whashington, DC.

Allen, T. M., Christopher, B.R., Elias, V.E., and DiMaggio, J. 2001 Developement of the simplified method for internal stability design of mechanically stabilized earth (MSE) walls. Whashington State Dept. Of Transportation Research Report. WA-RD 513.1, 108 p..

Allen, T. M., Bathurst, R.J., Berg, R.R. 2002. Global Level of Safety and Performance of Geosynthetic Walls: An Historical Perspective. Geosynth. Int., 9(5-6), p. 395-450.

Allen, T. M., Bathurst, R. J., Holtz, R. D., Walters, D. L. & Lee, W. F.. 2003. A new working stress method for prediction of reinforcement loads in geosynthetic walls. Can. Geotech. J., 40 (5), p. 976-994.

Bathurst, R. J., Huang, B., Allen, T. M. 2012. LRFD Calibration of the Ultimate Pullout Limit State for Geogrid Reinforced Soil Retaining Walls. Int. J. Geomech., 12(4), p. 399-413

Brinkgreve, R.B.J., Swolfs, W.M. & Engin, E. 2011. Plaxis Manual.

Cai, Z., and Bathurst, R.J.. 1995. Seismic response analysis of geosynthetic reinforced soil segmental retaining walls by finite element method. Comp. and Geotech., 17, p. 523-546.

Gottardi, G., Gragnano, C.G. & Tonni, L. 2014. Use of an advanced elasto-plastic model in the numerical analysis of a small-scale geosynthetic-reinforced wall from centrifuge tests, Proc. 10th Int. Conference on Geosynthetics, Berlin, Germany.

Hatami, K. and Bathurst, R.J.. 2005. Development and verification of a numerical model fort he analysis of geosynthetic-reinforced soil segmental walls under working stress. Can. Geotech. J., 42, p. 1066-1085.

Huang, B., Bathurst, R.J. and Hatami, K.. 2009. Numerical study of reinforcemed soil segmental walls using three different constitutive soil models. J. Geotech. Geoenviron. Eng., 135 (10), p. 1486-1498.

Iacorossi, M. 2012. Centrifuge modelling of earth-reinforced retaining walls. Master degree thesis, University of Bologna.

Iacorossi, M., Ling. H.I., Gottardi, G. & Li, L. 2013. Centrifuge modelling of earth-reinforced retaining walls. Proc. Int. Symp. on Design and Practice of Geosynthetic-Reinforced Soil Structures, Bologna, Italy, p. 3-12

Jacobs, F., Ziegler, M., Vollmert, L., Ehrenberg, H. 2014. Explicit design of geogrids with non linear interface model. Proc. 10th Int. Conference on Geosynthetics, Berlin, Germany.

Ling, H. I. & Leshchinsky, D. 2003. Parametric studies of the behaviour oft he segmental block reinforced soil retaining walls. Geosynth. Int., 10(3), p. 77-94.

Ling, H.I. & Liu, H. 2009. Deformations analysis of reinforced soil retaining walls – simplistic versus sophisticated finite element analyses. Acta Geotech, 4, p. 203-213.

Moraci, N., Gioffrè, D. 2006 A simple method to evaluate the pullout resistance of extruded geogrids embedded in a compacted granular soil. Geotext. Geomembr., 24, p. 116-128.

National Highway Institute, 2009. Design and construction of mechanically stabilized earth walls and reinforced soil slopes. Vol. I. U.S. Department of Transportation.

Schanz, T., Vermeer, P.A., Schanz, T. 1999. The hardening soil model: formulation and verification. In: Beyond 2000 in computational geotechnics – 10 years of Plaxis.

Siera, A.C.C.F., Gerscovich, D.M.S., Sayão A.S.F.J. 2009. Displacement and load transfer mechanisms of geogrid under pull-out condition. Geotext. Geomembr., 27, p. 241-253.

Yang, X. & Annamraju, S. 2013. Numerical analysis of cellular geosynthetic-reinforced soil using a Hypoplastic constitutive model. Proc. Int. Symp. on Design and Practice of Geosynthetic-Reinforced Soil Structures, Bologna, Italy, p. 449-457.

Yu, Y., Damians, I.P. and Bathurst, R.J. 2015. Influence of choice of FLAC and PLAXIS interface models on reinforced soil-structure interactions. Comp. Geotech., 65, p. 164-174.

Yu, Y., Bathurst, R.J. and Allen, T.M. 2016. Numerical modeling of the SE-18 geogrid reinforced modular block retaining walls. J. Geotech. Geoenviron. Eng., 10.1061/(ASCE)GT.1943-5606.0001438, 04016003.